

Singular and Half-Quantum Vortices and Associated Majorana Particles in Superfluid $^3\text{He-A}$ between Parallel Plates

Takuto KAWAKAMI*, Yasumasa TSUTSUMI, and Kazushige MACHIDA

Department of physics, Okayama University, Okayama 700-8530

(Received November 6, 2018)

Motivated by a recent experiment on superfluid $^3\text{He-A}$ confined in narrow parallel plates using a rotating cryostat, we explore possible vortices stable under magnetic field applied to arbitrary angle relative to the plates in order to seek vortices which can accommodate the Majorana zero mode in the core. After proving that the singular vortex with the unit winding number provides the Majorana mode in the spinful situation, we establish the phase diagram in the plane; the rotation frequency Ω vs system size R by finding possible order parameter textures within the Ginzburg-Landau framework. We also analyze the stability for a single and a pair of half-quantum vortices, which possesses the Majorana mode in its core. It is concluded from the above mention that the Majorana zero mode can be found in the present on-going experimental setting at ISSP, Univ. Tokyo.

KEYWORDS: ^3He , A-phase, chiral p -wave pairing, superfluid, parallel plate geometry, vortex, texture

1. Introduction

There has been much attention on topological orders and the associated Fermionic quasi-particles with low energies.¹⁻⁴⁾ This is particularly true when the quasi-particles are Majorana⁵⁾ character, namely its creation operator γ^\dagger is equal to its annihilation operator γ ; $\gamma^\dagger = \gamma$. This unusual and intriguing Fermion, quite different from the usual Dirac particle, is thought to be useful for fault-tolerant quantum computations because it obeys non-Abelian statistics⁶⁾ and its existence is protected topologically to avoid decoherence. These situations are ideal for quantum computation.⁷⁾ The candidate systems, which support the Majorana particle, are quite rare; chiral spinless $p_x \pm ip_y$ superconductors, p -wave Feshbach resonanced superfluid,⁸⁾ and the fractional quantum Hall state with the $5/2$ filling. The former superconductors have not been identified yet in nature. It has often been argued that Sr_2RuO_4 may be a prime candidate,¹⁰⁻¹³⁾ but strong doubt has been cast on this possibility of Sr_2RuO_4 of its triplet pairing.¹⁴⁻¹⁶⁾ Note that the first discovered triplet superconductor UPt_3 is an f -wave pairing, not chiral p -wave.¹⁷⁻¹⁹⁾ It is proven theoretically that the half-quantum vortex (HQV) in the chiral superconductors with the p -wave pairing possesses the Majorana particle with zero energy localized at the vortex core.^{20, 21)}

Superfluid $^3\text{He-A}$ phase is characterized by a chiral p -wave pairing. There is no doubt on this identification.^{22, 23)} In fact, Volovik and Mineev²⁴⁾ are the first to point out the possibility to the realization of HQVs in 1976. Since then, there have been several general arguments on the stability of a HQV in connection with $^3\text{He-A}$ phase.²⁵⁻²⁸⁾ However, there are no serious calculations which consider it in a realistic situation in superfluid $^3\text{He-A}$ phase on how to stabilize it and on what boundary conditions are needed for it.

Recently, Yamashita, *et al.*²⁹⁾ have performed an ex-

periment intended to observe HQVs in superfluid $^3\text{He-A}$ in parallel plate geometry. The superfluid is confined in a cylindrical region with the radius $R = 1.5$ mm and the height $12.5 \mu\text{m}$ sandwiched by parallel plates. A magnetic field $H = 26.7$ mT ($\parallel z$) is applied perpendicular to the parallel plates under pressure $P=3.05$ MPa. Since the gap $12.5 \mu\text{m}$ between plates is narrow compared to the dipole coherence length $\xi_d \sim 10 \mu\text{m}$, the l -vector, which signifies the direction of orbital angular momentum of Cooper pairs, is always perpendicular to the plates. Also the d -vector is confined within the plane by an applied field $H \parallel z$ because the dipole magnetic field $H_d \sim 2.0$ mT,^{22, 23)} where H tends to align the d -vector perpendicular to the field direction. They investigate to seek out various parameter spaces, such as temperature T , or the rotation speed Ω up to $\Omega = 6.28$ rad/sec by using the rotating cryostat in ISSP, Univ. Tokyo, capable for the maximum rotation speed ~ 12 rad/sec, but there is no evidence for the existence of the HQV.²⁹⁾

The aims in this paper are to investigate the possible vortex structures which can accommodate the Majorana particle in the core under the above realistic experimental situations at ISSP for superfluid $^3\text{He-A}$ phase confined in the parallel plates. The candidate vortex structures in this situation are either the singular vortex (SV) with odd winding number or HQVs mentioned above. Thus after examining the sufficient condition for the Majorana zero energy particle to exist in the SV, we determine the phase diagram in the system size with the radius R and the external rotation frequency Ω under applied fields with arbitrary angle relative to the plates. Note that the external field is necessary for performing NMR detection.²⁹⁾

The arrangement of the paper is as follows: In §2 we examine the possible order parameters and its spatial structures, or textures. By utilizing general symmetry properties of the superfluid $^3\text{He-A}$ phase, we demonstrate that the SV with odd winding number even in the spinful situation can accommodate the Majorana zero mode in

*E-mail address: kawakami@mp.okayama-u.ac.jp

	$w_{\uparrow\uparrow,+}$	$w_{\uparrow\downarrow,+}$	$w_{\downarrow\downarrow,+}$	$w_{\uparrow\uparrow,-}$	$w_{\uparrow\downarrow,-}$	$w_{\downarrow\downarrow,-}$
AT	0	0	0	2	2	2
SV	1	1	1	3	3	3
HQV	0	×	1	2	×	3

Table I. The combination of phase windings of each OP component for the A-phase texture (AT), the singular vortex (SV) and the half-quantum vortex (HQV).

the core. In §3 we investigate the stable vortices and textures within the Ginzburg-Landau (GL) formalism when the magnetic field is applied to an arbitrary angle relative to the plates, in order to find the stable SV region for various system parameters, external rotation Ω , the system size R and the field orientation θ_H . In §4 the stability problem of the single HQV and a pair of HQVs are analyzed within the same framework. We devote to summary and conclusions in the final section.

A part of the §4 is published in ref. 30.

2. General Considerations

2.1 Order parameters and textures

Generally, in p -wave superfluids, the order parameter (OP) is described by

$$\hat{\Delta}(\mathbf{r}, \hat{\mathbf{p}}) = \begin{pmatrix} \Delta_{\uparrow\uparrow}(\mathbf{r}, \hat{\mathbf{p}}) & \Delta_{\uparrow\downarrow}(\mathbf{r}, \hat{\mathbf{p}}) \\ \Delta_{\downarrow\uparrow}(\mathbf{r}, \hat{\mathbf{p}}) & \Delta_{\downarrow\downarrow}(\mathbf{r}, \hat{\mathbf{p}}) \end{pmatrix}. \quad (1)$$

The matrix element is described by

$$\begin{aligned} \Delta_{\sigma\sigma'}(\mathbf{r}, \hat{\mathbf{p}}) &= A_{\sigma\sigma',+}(\mathbf{r})\hat{p}_+ + A_{\sigma\sigma',-}(\mathbf{r})\hat{p}_- \\ &\quad + A_{\sigma\sigma',z}(\mathbf{r})\hat{p}_z, \end{aligned} \quad (2)$$

where σ is spin index \uparrow or \downarrow , $\hat{p}_\pm = \mp(\hat{p}_x \pm i\hat{p}_y)/\sqrt{2}$, and $\hat{\mathbf{p}}$ is the unit vector in the momentum space. In the parallel plate geometry, the momentum \hat{p}_z component is suppressed. Here each component $A_{\sigma\sigma',\pm}(\mathbf{r})$ ($\sigma = \uparrow, \downarrow$) can have its own phase winding whose winding number is denoted by $w_{\sigma\sigma',\pm}$. There are three possible textures at rest and under rotation as shown in Table I: ($w_{\sigma\sigma',+}, w_{\sigma\sigma',-}$) = (0, 2); A-phase texture (AT), (1, 3); SV, and ($w_{\uparrow\uparrow,+}, w_{\downarrow\downarrow,+}, w_{\uparrow\uparrow,-}, w_{\downarrow\downarrow,-}$) = (0, 1, 2, 3); HQV. These textures and vortices are allowed in axisymmetric situation (see §3.2). We investigate the detailed configuration of these textures, the relative energetics, and the associated Majorana quasi-particle in the last two textures.

2.2 Majorana bound state -symmetry considerations-

In this subsection, we examine the existence of the Majorana particle in the SV and the HQV in a most general situation. By assuming that the configurations of the OP are the bulk A-phase, the SV texture is described as

$$\begin{aligned} \Delta_{\sigma\sigma'}(\mathbf{r}, \hat{\mathbf{p}}) &= A_{\sigma\sigma',+}(\mathbf{r})\hat{p}_+ \\ &= d_{\sigma\sigma'}(\mathbf{r})A_+(r)\exp(i\phi)\hat{p}_+, \end{aligned} \quad (3)$$

where ϕ is the azimuthal angle of the center-of-mass coordinate \mathbf{r} ,

$$d_{\uparrow(\downarrow)}(\mathbf{r}) = \mp \frac{1}{\sqrt{2}}(d_x(\mathbf{r}) \mp id_y(\mathbf{r})),$$

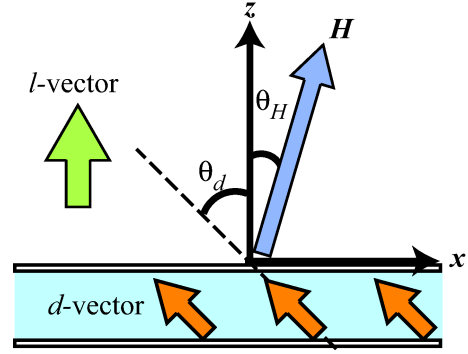


Fig. 1. (Color online) Schematic diagram of the parallel plate system. The external magnetic field \mathbf{H} tilts by θ_H from the z -axis. θ_d is the polar angle of the d -vector. The external field tends to align the d -vector perpendicular to \mathbf{H} and the dipole interaction tends to align the d -vector parallel to the direction z . Then $0 \leq \theta_d \leq \pi/2 - \theta_H$.

$$d_{\uparrow\downarrow}(\mathbf{r}) = d_z(\mathbf{r}),$$

and d -vector $\mathbf{d} = (d_x, d_y, d_z)$ is real. Under this assumption, the direction of d -vector is determined by the dipole interaction and the interaction with the external field. The polar and azimuthal angle of direction of d -vector are determined as

$$\theta_d^{(bulk)} = \frac{1}{2} \tan^{-1} \left[\frac{\sin 2\theta_H}{(H_d/H)^2 - \cos 2\theta_H} \right], \quad (4)$$

$$\phi_d^{(bulk)} = 0. \quad (5)$$

The angle θ_d and θ_H are defined as shown in Fig. 1. The angle ϕ_d is the azimuthal angle of the direction of d -vector. In other words, when the direction of the spin quantization axis is in the angle of $(\theta_d^{(bulk)} + \pi/2, \phi_d^{(bulk)})$, $d_{\uparrow\downarrow}(\mathbf{r}) = 0$ throughout the system.

When $\Delta_{\uparrow\downarrow}(\mathbf{r}_1, \mathbf{r}_2) = \Delta_{\downarrow\uparrow}(\mathbf{r}, \hat{\mathbf{p}}) = 0$, p -wave mean field Hamiltonian is written as

$$\mathcal{H} = \int d\mathbf{r}_1 d\mathbf{r}_2 \Psi^\dagger(\mathbf{r}_1) \begin{pmatrix} \hat{\mathcal{K}}_{\uparrow\uparrow} & 0 \\ 0 & \hat{\mathcal{K}}_{\downarrow\downarrow} \end{pmatrix} \Psi(\mathbf{r}_2), \quad (6)$$

where

$$\Psi(\mathbf{r}) = [\psi_\uparrow(\mathbf{r}), \psi_\uparrow^\dagger(\mathbf{r}), \psi_\downarrow(\mathbf{r}), \psi_\downarrow^\dagger(\mathbf{r})]^T,$$

$$\hat{\mathcal{K}}_{\sigma\sigma} = \begin{bmatrix} H_0^\sigma(\mathbf{r}_1, \mathbf{r}_2) & \Delta_{\sigma\sigma}(\mathbf{r}_1, \mathbf{r}_2) \\ -\Delta_{\sigma\sigma}^*(\mathbf{r}_1, \mathbf{r}_2) & -H_0^{\sigma*}(\mathbf{r}_1, \mathbf{r}_2) \end{bmatrix},$$

$$\begin{aligned} H_0^{(\sigma)}(\mathbf{r}_1, \mathbf{r}_2) &= \left[-\frac{\nabla_1^2}{2m_3} + V(\mathbf{r}_1) - \mu_\sigma \right. \\ &\quad \left. + i\Omega \left(x_1 \frac{\partial}{\partial y_1} - y_1 \frac{\partial}{\partial x_1} \right) \right] \delta(\mathbf{r}_1 - \mathbf{r}_2), \end{aligned}$$

where m_3 , V , and μ_σ are the mass of the ^3He atom, the single particle potential, and the chemical potential of the particle whose spin σ . We carry out the Bogoliubov transformation to quasi particles whose creation and annihilation operators

$$\eta_{\nu\uparrow} = \int d\mathbf{r} [u_{\nu 1}^*(\mathbf{r})\psi_{\uparrow}(\mathbf{r}) + u_{\nu 2}^*(\mathbf{r})\psi_{\downarrow}(\mathbf{r}) + v_{\nu 1}^*(\mathbf{r})\psi_{\uparrow}^\dagger(\mathbf{r}) + v_{\nu 2}^*(\mathbf{r})\psi_{\downarrow}^\dagger(\mathbf{r})], \quad (7)$$

$$\eta_{\nu\downarrow} = \int d\mathbf{r} [v_{\nu 1}(\mathbf{r})\psi_{\uparrow}(\mathbf{r}) + v_{\nu 2}(\mathbf{r})\psi_{\downarrow}(\mathbf{r}) + u_{\nu 1}(\mathbf{r})\psi_{\uparrow}^\dagger(\mathbf{r}) + u_{\nu 2}(\mathbf{r})\psi_{\downarrow}^\dagger(\mathbf{r})]. \quad (8)$$

Obtained Bogoliubov-de Gennes (BdG) equation is

$$\int d\mathbf{r}_2 \begin{bmatrix} \hat{\mathcal{K}}_{\uparrow\uparrow}(\mathbf{r}_1, \mathbf{r}_2) & 0 \\ 0 & \hat{\mathcal{K}}_{\downarrow\downarrow}(\mathbf{r}_1, \mathbf{r}_2) \end{bmatrix} \underline{\psi}_{\nu}(\mathbf{r}_2) = \underline{\psi}_{\nu}(\mathbf{r}_1) \begin{bmatrix} \hat{E}_{\nu}^{\uparrow} & 0 \\ 0 & \hat{E}_{\nu}^{\downarrow} \end{bmatrix}, \quad (9)$$

where $\hat{E}_{\nu}^{\sigma} = \sigma_3 E_{\nu}^{\sigma}$. This σ_3 is the Pauli matrix. We can reduce the BdG equation (9) to four eigenvalue equations,

$$\int d\mathbf{r}_2 \hat{\mathcal{K}}_{\uparrow\uparrow}(\mathbf{r}_1, \mathbf{r}_2) \begin{pmatrix} u_{\nu 1}(\mathbf{r}_2) \\ v_{\nu 1}(\mathbf{r}_2) \end{pmatrix} = \text{sgn}(\sigma) E_{\nu}^{\sigma} \begin{pmatrix} u_{\nu 1}(\mathbf{r}_1) \\ v_{\nu 1}(\mathbf{r}_1) \end{pmatrix}, \quad (10)$$

$$\int d\mathbf{r}_2 \hat{\mathcal{K}}_{\downarrow\downarrow}(\mathbf{r}_1, \mathbf{r}_2) \begin{pmatrix} u_{\nu 2}(\mathbf{r}_2) \\ v_{\nu 2}(\mathbf{r}_2) \end{pmatrix} = \text{sgn}(\sigma) E_{\nu}^{\sigma} \begin{pmatrix} u_{\nu 2}(\mathbf{r}_1) \\ v_{\nu 2}(\mathbf{r}_1) \end{pmatrix}. \quad (11)$$

These eigenvalue equations are solved numerically.³¹⁾ If $\Delta_{\sigma\sigma}(\mathbf{r}, \hat{\mathbf{p}})$ has odd phase winding, we can obtain the zero energy state ($E_{\nu}^{\sigma} = 0$) and $(u_{\nu,i}(\mathbf{r}), v_{\nu,i}(\mathbf{r})) = (v_{\nu,i}^*(\mathbf{r}), u_{\nu,i}^*(\mathbf{r}))$ so that $\eta_{\nu\sigma} = \eta_{\nu\sigma}^{\dagger}$. That is, the Bogoliubov quasi-particles exhibit the Majorana character.

In the SV texture all components of the OP have the odd winding number. Thus the SV has the Majorana quasi-particle with the external field toward any direction. In the HQV texture, either $\Delta_{\uparrow\uparrow}(\mathbf{r}, \hat{\mathbf{p}})$ or $\Delta_{\downarrow\downarrow}(\mathbf{r}, \hat{\mathbf{p}})$ has the odd phase winding. The component that has no phase windings does not have the lower excitation. That is, the HQV has the lower excitation that is induced by the odd phase winding and these excitations contain the Majorana quasi-particle. Consequently, both the SV and the HQV have the Majorana quasi-particle at these vortex cores.

However, in the above analysis, we do not consider the influence of the vortex core and the edge of system. In these situation, the configuration of the OP is different from the bulk A-phase due to variance of the OP, mixture of minor components, and so on. Furthermore, the Majorana quasi-particle exists at the vortex core and the edge of system. Then we have to clarify OP textures by more realistic and serious calculation using GL theory.

3. Ginzburg-Landau Functional and Phase Diagram

3.1 Ginzburg-Landau functional

The GL free-energy functional invariant under gauge transformation, spin, and orbital space rotations is well established^{22, 23, 27, 32-37)} and given by a standard form

$$f_{total} = f_{grad} + f_{bulk} + f_{dipole} + f_{field}, \quad (12)$$

$$f_{grad} = K [(\partial_i^* A_{\mu j}^*)(\partial_i A_{\mu j}) + (\partial_i^* A_{\mu j}^*)(\partial_j A_{\mu i}) + (\partial_i^* A_{\mu i}^*)(\partial_j A_{\mu i})],$$

$$f_{bulk} = -\alpha_{\uparrow\uparrow} A_{\uparrow\uparrow, i}^* A_{\uparrow\uparrow, i} - \alpha_{\uparrow\downarrow} A_{\uparrow\downarrow, i}^* A_{\uparrow\downarrow, i} - \alpha_{\downarrow\downarrow} A_{\downarrow\downarrow, i}^* A_{\downarrow\downarrow, i} + \beta_1 A_{\mu i}^* A_{\mu i}^* A_{\nu j} A_{\nu j} + \beta_2 A_{\mu i}^* A_{\nu j}^* A_{\mu i} A_{\nu j} + \beta_3 A_{\mu i}^* A_{\nu i}^* A_{\mu j} A_{\nu j} + \beta_4 A_{\mu i}^* A_{\nu j}^* A_{\mu j} A_{\nu i} + \beta_5 A_{\mu i}^* A_{\mu j}^* A_{\nu i} A_{\nu j},$$

$$f_{dipole} = g_d (A_{\mu\mu}^* A_{\nu\nu} + A_{\mu\nu}^* A_{\nu\mu} - \frac{2}{3} A_{\mu\nu}^* A_{\mu\nu}),$$

$$f_{field} = g_m H_{\mu} A_{\mu i}^* H_{\nu} A_{\nu i},$$

where $\mu, i = x, y, z$ and $\partial_i = \nabla_i - (2im_3/\hbar)(\mathbf{\Omega} \times \mathbf{r})_i$ ($\mathbf{\Omega} \parallel \mathbf{z}$) with m_3 being the mass of the ^3He atom. The coefficients of quadratic terms

$$\alpha_{\sigma\sigma'} = \alpha_0 (1 - T/T_c + \text{sgn}(\sigma + \sigma') \Delta T/T_c), \quad (13)$$

where $\alpha_0 = N(0)/3$. The Zeeman effect splits the transition temperature $T_{c\uparrow}$ of the $|\uparrow\uparrow\rangle$ pair and $T_{c\downarrow}$ of the $|\downarrow\downarrow\rangle$ pair.³⁸⁾ The split width $\Delta T \equiv (T_{c\uparrow} - T_{c\downarrow})/2$ in eq. (13). However, we consider the region that $\Delta T \ll T_c - T$ so-called weak field region until §4. The coefficient of fourth order terms β_i ³⁹⁾ are obtained in ref. 33 appropriate for the experiment at $P = 3.05$ MPa. We use the gradient coupling constant with weak coupling limit $K = 7\zeta(3)N(0)(\hbar v_F)^2/240(\pi k_B T_c)$. The g_d ³⁵⁾ and the g_m are the coupling constant of the dipole interaction and the interaction with external field respectively,

$$g_d = \frac{\mu_0}{40} \left[\gamma \hbar N(0) \ln \frac{1.1339 \times 0.45 T_F}{T_c} \right], \quad (14)$$

$$g_m = \frac{7\zeta(3)N(0)(\gamma \hbar)^2}{48[(1 + F_0^a)\pi k_B T_c]}. \quad (15)$$

The transition temperature under no magnetic field T_c , the density of states $N(0)$, Fermi velocity v_F , the permeability of vacuum μ_0 , the gyromagnetic ratio γ , Landau parameter F_0^a , and Fermi temperature T_F are given by experiments.^{32, 34)} In order to carry out realistic calculations taking account of the configuration of the vortex core and the edge of the system, our formulation includes strong coupling corrections in the bulk terms where the A-phase is stable over the B-phase. Thus the gradient terms are within the weak coupling limit ($\rho_{sp}/\rho_s = 1$) because there is no established method to properly take into account the Fermi liquid correction for the OP form generalized beyond the A-phase (see for standard method ref. 23). We minimize the GL functional eq. (12) where

the external field is applied to arbitrary direction relative to the plates and absolute value. First, we consider two limits where the direction of the external magnetic field is parallel and perpendicular to the plates.

3.2 Parallel field H_{\parallel}

In the situation where the external field applies parallel to the plates, both the dipole interaction and the external field suppresses the components of the OP $\Delta_{\uparrow\uparrow}(\mathbf{r})$ and $\Delta_{\downarrow\downarrow}(\mathbf{r})$. In the bulk A-phase system, the two components $A_{\uparrow\downarrow,\pm}(\mathbf{r})$ survive. Since the phase winding of the OP components increases the kinetic energy of Cooper pairs, it is energetically favorable at rest that large component of the OP has small winding number. Furthermore, in the cylindrical symmetric system, $w_{\uparrow,+} = w_{\uparrow,-} - 2$ due to orbital coupling effect.³⁰⁾ Under low rotations the stable texture is the AT whose phase winding $(w_{\uparrow,+}, w_{\uparrow,-}) = (0, 2)$ and the dominant component of the OP is $A_{\uparrow,+}(\mathbf{r})$.

Under the anti-clock wise rotation the component that has the positive phase winding gains the rotating energy through a term $-w_{\uparrow\pm}|A_{\uparrow\pm}|^2$ in the GL functional eq. (12). As the rotating speed Ω is higher, the free energy of the SV whose dominant component of the OP has winding number $w = 1$ becomes lower than that of the AT. According to the above analysis, the candidates of stable SVs are $(w_{\uparrow,+}, w_{\uparrow,-}) = (-1, 1)$ and $(1, 3)$. The $(-1, 1)$ texture has smaller winding number than the $(1, 3)$ texture, from the kinetic energy view point the $(-1, 1)$ texture seems to be more stable than the $(1, 3)$. However, under rotation the minor component $A_{\uparrow,-}(\mathbf{r})$ of $(1, 3)$ texture gains more rotating energy than the minor component $A_{\uparrow,+}(\mathbf{r})$ of $(-1, 1)$ texture. Under rotation the stable texture is determined by competition of those two factors. The results of our calculation show that when the rotating speed is large enough to stabilize the SV not AT, $(1, 3)$ texture is always more stable than $(-1, 1)$ texture.

In Fig. 2, the cross section of the amplitude of the OP component of the AT and the SV when the direction of the external field is parallel to the plates and the quantization axis of spin is chosen perpendicular to the plates. Choosing the quantization axis parallel to the plates same as the direction of the field, we can obtain the SV texture whose OP component $\Delta_{\uparrow\downarrow}(\mathbf{r}) = 0$ exactly. The SV texture has Majorana quasi-particle state at the vortex core.

The phase diagram of textures in the space consisting of the rotating speed Ω and system size R is shown in Fig. 3 in a fixed temperature $T/T_c = 0.95$. We calculate in various temperatures and absolute values of external field, showing that the temperature and the absolute value of external field change Ω_c only slightly, so that Ω_c is determined by almost only R . We obtain the critical rotating speed Ω_c quantitatively as a function of system size R smaller than $100 \mu\text{m}$. Therefore, we can extrapolate $\Omega_c = 0.06 \text{ rad/sec}$ in $R = 1.5 \text{ mm}$, that is the system size of the sample using the experiment in ISSP. This rotating speed can be well controlled by the present experimental technique.

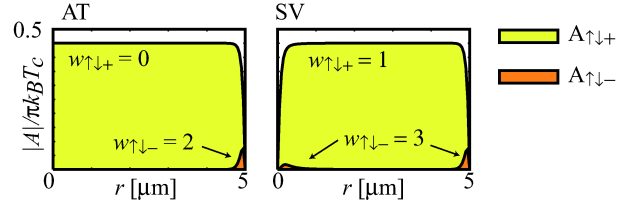


Fig. 2. (Color online) Order parameter amplitude $|A_{\sigma\sigma',\pm}|$ normalized by $\pi k_B T_c$. Left (right) figure shows the cross section of the OP components along the radial direction \mathbf{r} of the AT (SV) texture for $R = 5 \mu\text{m}$, $T/T_c = 0.95$, $H = 10 \text{ mT}$, $\theta_H = \pi/2$. We choose the spin quantization axis perpendicular to the plates; the \mathbf{z} direction. The spin component $\Delta_{\sigma\sigma}$ vanishes.

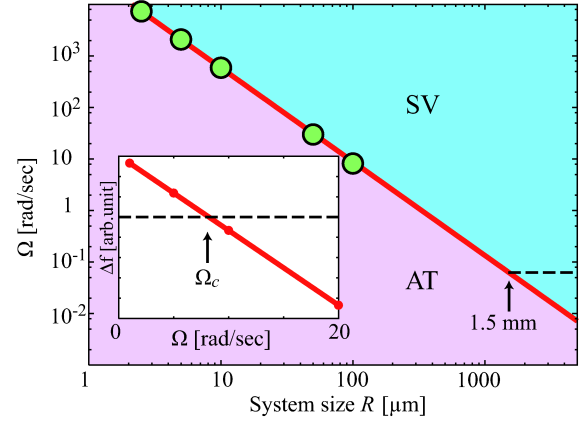


Fig. 3. System size R dependence of the critical angular velocity Ω_c from the AT to the SV $T/T_c = 0.95$, $\mathbf{H} \parallel$ plates ($\theta_H = \pi/2$). An extrapolated value of $\Omega_c = 0.06 \text{ rad/sec}$ is found at $R = 1.5 \text{ mm}$. The inset shows the energy differences Δf between the two textures as a function of Ω for $R = 100 \mu\text{m}$.

3.3 Perpendicular field H_{\perp}

In this subsection we consider the situation where the external field apply parallel to the plates. When the external field larger than the dipole field H_d , the d -vectors lie parallel to the plates. The result of numerical calculation shows that $\Delta_{\uparrow\downarrow}(\mathbf{r}, \hat{\mathbf{p}}) = 0$ exactly throughout the system as shown in Fig. 4. These SV textures have the Majorana quasi-particle state at the vortex core. When the external field is smaller than the dipole field H_d , in the bulk A-phase the d -vector aligns perpendicular to the plates. The OP texture is same as in the case that the external field is parallel to the plates shown in Fig. 2. Choosing the quantization axis parallel to the plates, we can obtain the OP component $\Delta_{\uparrow\downarrow}(\mathbf{r}) = 0$ exactly. However, when d -vector $\parallel \mathbf{H}$ taking account of Zeeman effect in BdG equation (9), the symmetry of the equation arrows the solution $(u_{\nu,1}(\mathbf{r}), v_{\nu,1}(\mathbf{r})) = (v_{\nu,2}^*(\mathbf{r}), u_{\nu,2}^*(\mathbf{r}))$. Thus the core bound state of the SV cannot satisfy Majorana condition $(u_{\nu,i}(\mathbf{r}), v_{\nu,i}(\mathbf{r})) = (v_{\nu,i}^*(\mathbf{r}), u_{\nu,i}^*(\mathbf{r}))$. Therefore only in the case where the external field is larger than the dipole field H_d , the stabilized SV has the Majorana quasi-particle.

The phase diagram of textures are same as that in §3.2 since in the result of our calculation, the external magnetic field change critical rotating speed Ω_c of the

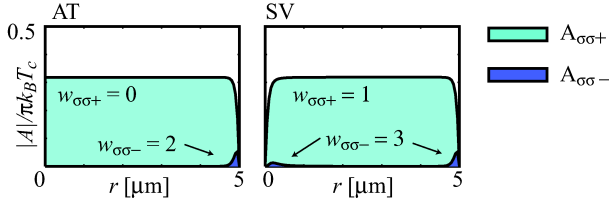


Fig. 4. (Color online) Order parameter amplitude $|A_{\sigma\sigma',\pm}|$ normalized by $\pi k_B T_c$ for $R = 5 \mu\text{m}$, $T/T_c = 0.95$, $H = 10 \text{ mT}$, $\theta_H = 0$. Left (right) figure shows the cross section of the OP components along the radial direction r of the AT (SV) texture. We choose the spin quantization axis perpendicular to the plates; z direction. The spin component $\Delta_{\uparrow\downarrow}(\mathbf{r}, \hat{\mathbf{p}}) = 0$ exactly.

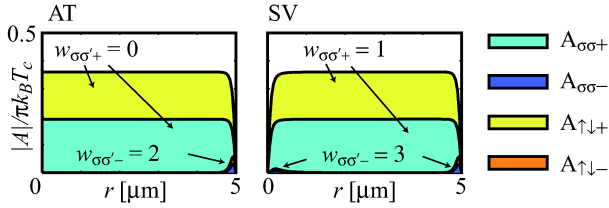


Fig. 5. (Color online) Order parameter amplitude $|A_{\sigma\sigma',\pm}|$ normalized by $\pi k_B T_c$ for $R = 5 \mu\text{m}$, $T/T_c = 0.95$, $H = 2 \text{ mT}$, $\theta_H = \pi/18$. Left (right) figure shows the cross section of the OP components along the radial direction r of the AT (SV) texture. We choose the spin quantization axis perpendicular to the plates; z direction. All spin components $\Delta_{\sigma\sigma'}(\mathbf{r}, \hat{\mathbf{p}})$ are non-vanishing. When we choose the spin quantization axis to be the direction $\theta = \theta_d^{(bulk)} + \pi/2$ and $\phi = 0$, $A_{\uparrow\downarrow,\pm} \ll A_{\sigma\sigma,\pm}$.

texture transition from the AT to the SV only slightly as shown in §3.4.

In the case that $\mathbf{H} \perp$ plates where the external field is larger than the dipole field H_d , the d -vector is perpendicular to the l -vector. Then the dipole energy of the bulk system can be neglected. Thus this case is favorable for realization of the HQV texture. We discuss the HQV texture in §4 in detail.

3.4 Arbitrary oriented field

In the bulk A-phase system, the direction of the d -vector is determined by the competition between the dipole interaction favoring that the d -vector is parallel to l -vector and the external field favoring that the d -vector is perpendicular to the \mathbf{H} . The direction of the d -vector is given by eqs. (4) and (5). When the quantization axis is perpendicular to the plates, all components $\Delta_{\sigma\sigma'}(\mathbf{r}, \hat{\mathbf{p}})$ are non-vanishing as shown in Fig. 5.

We consider the energetics of these textures by calculating the stable textures under various external magnetic fields; $H = 1, 2, 3$, and 10 mT , for various polar angles $\theta_H = n\pi/18$ $n = 1, 2, \dots$. The result of the calculation in the system $R = 5 \mu\text{m}$ which is shown in Fig. 6. Under these external fields, Ω_c coincides with each other for the precision in second order after the decimal point. We see that the external magnetic field scarcely changes the phase diagram shown in Fig. 3. Their reasons are as follows. The critical rotation Ω_c is determined by the competition of the kinetic energy and the energy gain

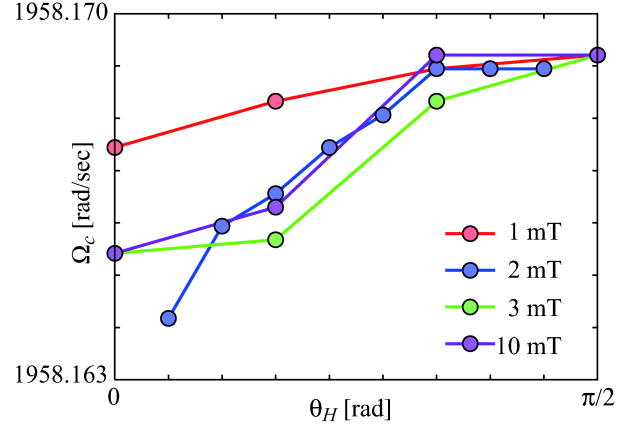


Fig. 6. (Color online) The critical angular velocity Ω_c dependence of θ_H from the AT to the SV for $T/T_c = 0.95$, $R = 5 \mu\text{m}$, $H = 1, 2, 3$, and 10 mT . Under the various direction and absolute value of the external fields, Ω_c coincides with each other for the precision in second order after the decimal point.

from angular momentum, namely, the gradient term. On the other hands the influence of the interaction with the external field is no more than 10^{-6} order of the gradient energy.

We discuss the possibility that the Majorana quasi-particle exists in these textures. As shown in §2.2, the SV has the Majorana quasi-particle when their OP component $\Delta_{\uparrow\downarrow}(\mathbf{r}, \hat{\mathbf{p}}) = 0$ for appropriate quantization axis throughout the system. Thus we turn the quantization axis to be their polar and azimuthal angle $(0, 0) \mapsto (\theta_d^{(bulk)} + \pi/2, \phi_d^{(bulk)})$ in order to change the expression to that suppressing the component of the OP $\Delta_{\uparrow\downarrow}(\mathbf{r}, \hat{\mathbf{p}})$. Then we obtain changed OP textures as shown in Fig. 7. In these textures, the components of the OP $A_{\uparrow\downarrow,\pm}(\mathbf{r}) \neq 0$, but finite amplitude with the order 10^{-3} against the dominant component $A_{\sigma\sigma\pm}(\mathbf{r})$. These amplitudes vary spatially, and their phase cannot be specified by the accurate A-phase OP. In addition, when the d -vector is not perpendicular to the magnetic field \mathbf{H} , we should note the influence of Zeeman effect for the Majorana condition. Therefore, we cannot conclude whether or not those SVs have the Majorana quasi-particle. In order to clarify these points, we have to solve spinful BdG equation include off-diagonal terms of eq. (9). These remain as a future problem.

We notice these induced components. In Fig. 8, we show the maximum value of amplitude of induced component $A_{\uparrow\downarrow,+}(\mathbf{r})$ as a function of θ_H in various external field values. We show that when the direction of the external field are perpendicular to the plates ($\theta_H = 0$) and parallel to the plates ($\theta_H = \pi/2$), the component $A_{\uparrow\downarrow,+}(\mathbf{r}) = 0$ exactly. Moreover, when the external field comparable to the dipole field H_d ($\simeq 2 \text{ mT}$), the induced component is enhanced maximally under such a magnitude of the field.

The system size dependence of them is shown in Fig. 9. When the system size becomes large, the amplitude of the component $A_{\uparrow\downarrow,+}(\mathbf{r})$ tend to be large. Therefore, even if the large sample such as that used in experiment

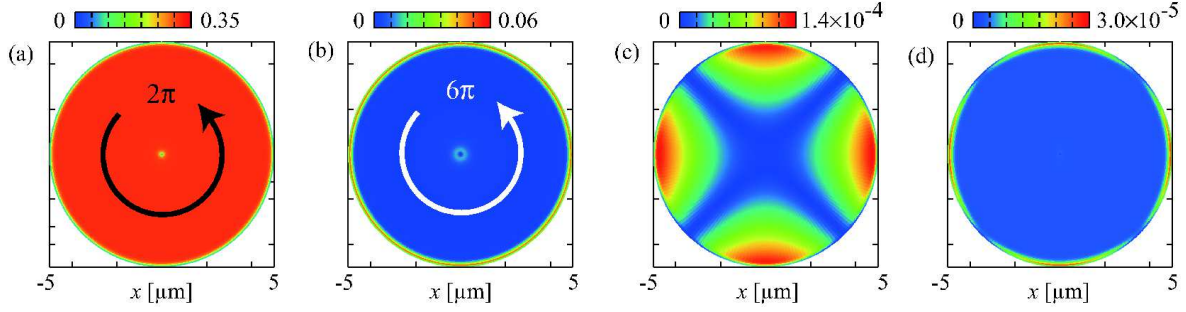


Fig. 7. (Color online) Order parameter amplitude (a) $|A_{\sigma\sigma,+}|$, (b) $|A_{\sigma\sigma,-}|$, (c) $|A_{\uparrow\downarrow,+}|$, and (d) $|A_{\uparrow\downarrow,-}|$ normalized by $\pi k_B T_c$ for $R = 5 \mu\text{m}$, $T/T_c = 0.95$, $H = 2 \text{ mT}$, $\theta_H = \pi/18$. We choose the spin quantization axis $\theta = \theta_d^{(bulk)} + \pi/2$, $\phi = 0$. The spin components $\Delta_{\uparrow\downarrow}(\mathbf{r}, \hat{\mathbf{p}}) \neq 0$ but have the amplitude with the order 10^{-3} of the amplitude of $\Delta_{\sigma\sigma}(\mathbf{r}, \hat{\mathbf{p}})$ and modulate spatially.

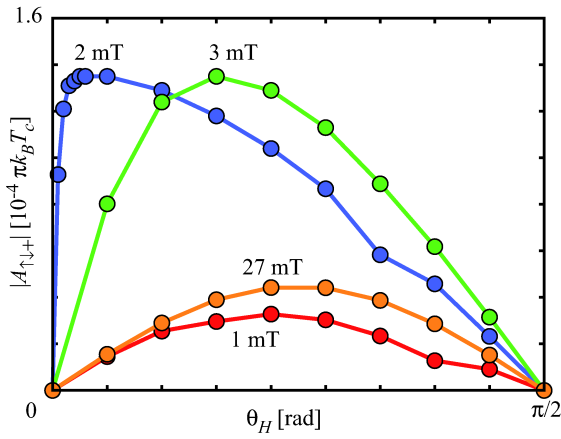


Fig. 8. (Color online) The maximum value of $|A_{\uparrow\downarrow,+}|$ as a function of θ_H for $H = 2, 3,$ and 27 mT , $R = 5 \mu\text{m}$, $T/T_c = 0.95$. When $\theta_H = 0$ or $\pi/2$, the amplitude of the component $\Delta_{\uparrow\downarrow}(\mathbf{r}, \hat{\mathbf{p}}) = 0$ exactly. When the external field is comparable to dipole field (≈ 2) mT, the amplitude of these components is enhanced.

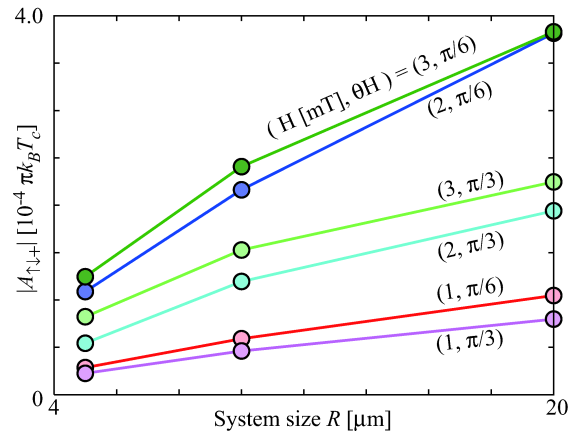


Fig. 9. The maximum value of $|A_{\uparrow\downarrow,+}|$ as a function of R for $H = 1, 2,$ and 3 mT , $\theta_H = \pi/6$ and $\pi/3 \text{ rad}$, μm , $T/T_c = 0.95$. When the system size becomes larger, the amplitude of these components becomes larger. In the system using experiment, $R = 1.5 \text{ mm}$, $|A_{\uparrow\downarrow,\pm}|$ are non-vanishing.

$R = 1.5 \text{ mm}$, these components are finite.

We suggest that the reason why the induced component is non-zero is due to the existence of induced $A_{\sigma\sigma',-}$ component. Taking account of the $A_{\sigma\sigma',-}$ component, the direction of d -vector determined by minimizing $f_{dipole} + f_{field}$ has the component parallel to the spin quantization axis except for the case that $\mathbf{H} \parallel$ plates and $\mathbf{H} \perp$ plates. In addition, these components varies spatially according to spatial modulation of $A_{\sigma\sigma',-}$ component.

4. Half-Quantum Vortex

4.1 Single half-quantum vortex

When the direction of the external field is perpendicular to the plates, it is a favorable situation for the HQV to realize. Then in this section, we consider possible stable HQV texture and their energetics. First, we consider the case that there is a single HQV in the system. The external magnetic field splits T_c of the $|\uparrow\uparrow\rangle$ and $|\downarrow\downarrow\rangle$ pairs by the Zeeman effect.³⁸⁾ The splitting is defined as $\Delta T = (T_{c\uparrow} - T_{c\downarrow})/2$. When $\Delta T > 0$ ($\Delta T < 0$), the amplitude of the OP $\Delta_{\uparrow\uparrow}$ ($\Delta_{\downarrow\downarrow}$) becomes larger than $\Delta_{\downarrow\downarrow}$ ($\Delta_{\uparrow\uparrow}$). The splitting ΔT is generally much smaller

than the amplitude of the OP in the so-called weak field region $H \approx 10 \text{ mT}$. In this region, the texture of the HQV are shown in Fig. 10. The rotation speed Ω_{c1} (Ω_{c2}) at which the free energy of the HQV (SV) and the AT (HQV) are intersect. In Fig. 11, we show that the HQV never becomes the absolute stable texture. The reasons are the strong coupling effect in the bulk fourth terms of GL functional eq. (12). In the weak coupling limit, under some critical rotation, the AT, the SV, and the HQV degenerate each other. The strong coupling effect stabilize the A phase, then the structure of the central region of the AT are more favorable than the others. Therefore, the critical rotation Ω_{c1} are larger than Ω_{c2} .

When the temperature becomes larger, the amplitude of the OP becomes smaller. Then the split ΔT cannot be neglected. When the split $\Delta T > 0$, the $|\uparrow\uparrow\rangle$ pair becomes dominant. Thus, the HQV texture and the energy difference Δf in Fig. 11 become close to the AT. In this process, Ω_{c1} become smaller than Ω_{c2} . Furthermore, when the temperature becomes larger, the stable region of the HQV becomes larger as shown in Fig. 12. Consequently, the phase diagram is shown in Fig. 13. We can extrapolate that the stability region of the HQV

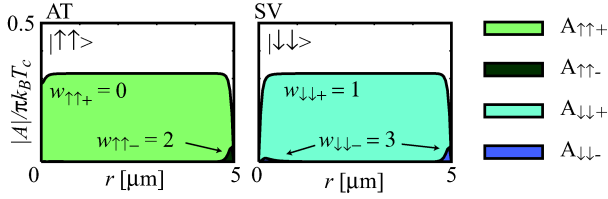


Fig. 10. (Color online) Order parameter amplitude of (a) $A_{\uparrow\uparrow,\pm}$ and (b) $A_{\downarrow\downarrow,\pm}$ components normalized by $\pi k_B T_c$ for $R = 5 \mu\text{m}$, $T/T_c = 0.95$, $H = 10 \text{ mT}$, $\theta_H = 0$. We choose the spin quantization axis perpendicular to the plates; z direction. At the vortex core, $A_{\uparrow\uparrow,\pm}$ component is only non-vanishing, so that the HQV is A_1 -core vortex.

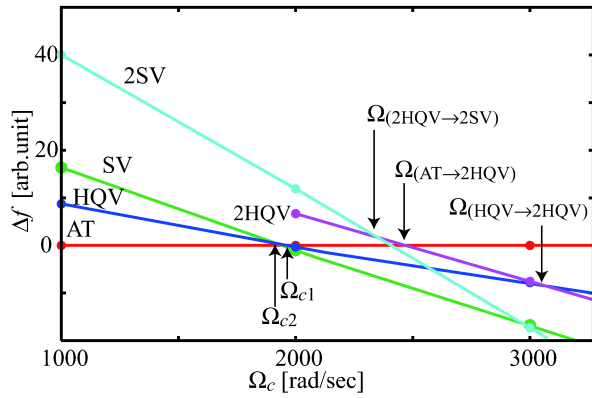


Fig. 11. (Color online) Free-energy comparison for the AT, the HQV, the SV, the two HQVs system (2HQV), and the two SVs system (2SV) as a function of Ω for $R = 10 \mu\text{m}$ and $T/T_c = 0.97$ at the weak field region. The Δf is the relative free energy to the AT. In the weak field region, $\Omega_{c2} < \Omega_{c1}$.

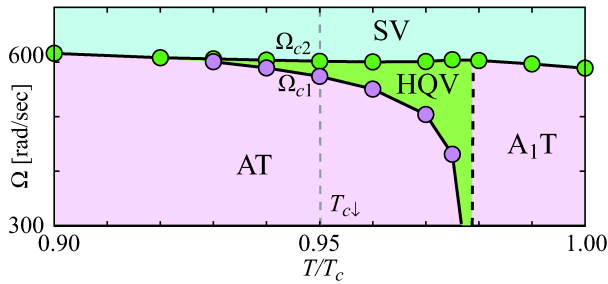


Fig. 12. (Color online) Stability region of the HQV in Ω versus T/T_c ($R = 10 \mu\text{m}$ and $\Delta T/T_c = 0.05$). A_1T denotes the A_1 phase texture where only $|\uparrow\uparrow\rangle$ pair exist. The stability region of the HQV becomes wide at the vicinity of the transition temperature from the A-phase to the A_1 -phase.

is $0.05 < \Omega < 0.06 \text{ rad/sec}$ in the sample whose size $R = 1.5 \text{ mm}$. We also notice that by changing the radius R of the system one can control the width of the stability region. For example, in $R = 100 \mu\text{m}$, the stability region of the HQV is $7 < \Omega < 8 \text{ rad/sec}$.

4.2 A pair of half-quantum vortices

We examine the case that there are more than two half-quantum vortices in the system. There are two possibilities to enter the two HQVs in the system. Namely,

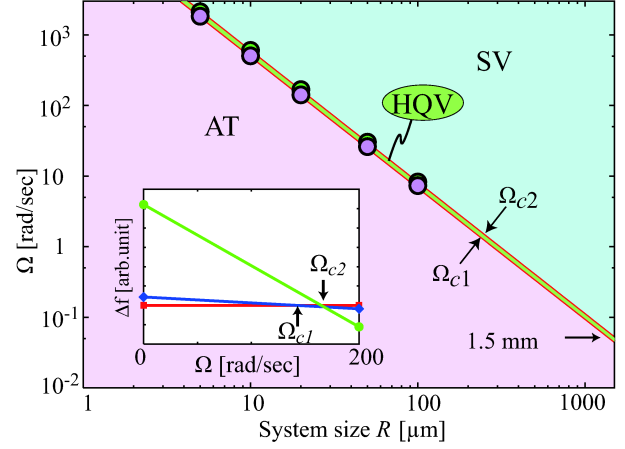


Fig. 13. Stability region of HQV sandwiched between Ω_{c1} and Ω_{c2} as a function of R for $T/T_c = 0.97$ and $\Delta T/T_c = 0.05$ ($H \simeq 100 \text{ mT}$). The critical rotation $\Omega_{c1} = 0.05 \text{ rad/sec}$ is the extrapolated value for $R = 1.5 \text{ mm}$. Inset shows the free-energy comparison for $R = 20 \mu\text{m}$, displaying the successive transitions from the AT to the HQV at Ω_{c1} and from the HQV to the SV at Ω_{c2} .

the one case is that there are the HQVs whose winding number $(w_{\uparrow\uparrow+}, w_{\downarrow\downarrow+}, w_{\uparrow\uparrow-}, w_{\downarrow\downarrow-}) = (0, 1, 0, 3)$ and $(1, 0, 3, 0)$ in the system, the other case is that there are two $(0, 1, 2, 3)$ -HQVs. We calculate these two cases and conclude that the former is not solution of our calculation. The center of phase winding of the component of the OP does not coincide with the center of the system, which is not the energetically advantageous form for the angular momentum. Furthermore, there is no repulsion between HQVs because we assume that the gradient energy are the weak coupling limit form.

We investigate the case that there are two $(0, 1, 2, 3)$ -HQVs in the system. In the Fig. 14 we show the texture of the two HQVs system (2HQV). In this texture, the component that has the phase winding are the same spin state. Thus the distance between them is determined by the competition of the kinetic energy loss and the energy gain from the angular momentum. However, we conclude these are just metastable texture from our calculation.

First of all, we consider the case that $\Delta T < 0$ where the $|\downarrow\downarrow\rangle$ pair is dominant. In this case, the texture of the 2HQV is close to two SVs system (2SV). From the analogy with the single HQV case, it can be guessed that critical rotation $\Omega_{(AT \rightarrow 2HQV)}$ where the free energy of the 2HQV cross to that of the AT is larger than the critical rotation $\Omega_{(2HQV \rightarrow 2SV)}$ where the free energy of the 2SV crosses to that of the AT. Namely, the 2HQV cannot be stable in this course.

On the other hands, we consider the case that $\Delta T > 0$ where the $|\uparrow\uparrow\rangle$ pair is dominant. In this case the texture of the 2HQV are energetically close to the AT. From the analogy with the single HQV case, it is possible that $\Omega_{(AT \rightarrow 2HQV)} < \Omega_{(2HQV \rightarrow 2SV)}$. However, in these regions, the SV is more stable than the AT. From our calculation, we show that the critical rotation speed $\Omega_{(HQV \rightarrow 2HQV)}$ where the free energy of the 2HQV crosses to that of the HQV cannot smaller than the critical rotation where

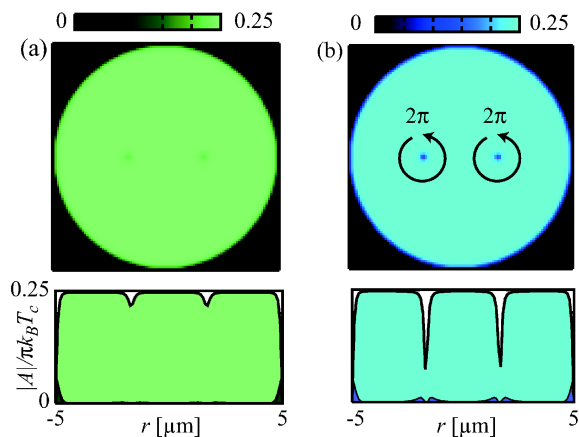


Fig. 14. (Color online) Order parameter amplitude (a) $A_{\uparrow,\pm}$ and (b) $A_{\downarrow,\pm}$ components normalized by $\pi k_B T_c$ for the metastable 2HQV system, $R = 5 \mu\text{m}$, $T/T_c = 0.95$, $\theta_H = 0$. We choose the spin quantization axis perpendicular to the plates; z direction. There are two vortices whose winding number 1 in the $|\downarrow\downarrow\rangle$ space. The sense of the phase winding and its number are shown. The low figures are cross sections of each component across the vortex cores.

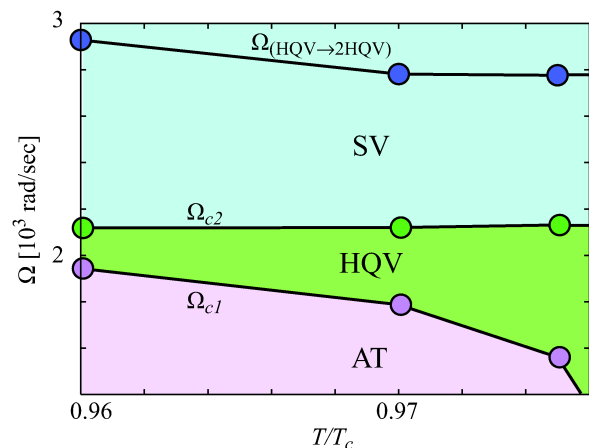


Fig. 15. Critical angular velocity $\Omega_{(\text{HQV} \rightarrow 2\text{HQV})}$ from the HQV to the 2HQV for $R = 5 \mu\text{m}$ and $\Delta T/T_c = 0.05$. Even if the temperature becomes higher, $\Omega_{(\text{HQV} \rightarrow 2\text{HQV})}$ does not become lower than Ω_{c2} .

the free energy of the SV crosses to that of the HQV as shown in Fig. 15. Namely the 2HQV cannot also be stable in this course.

5. Summary and conclusions

We have studied the relative stability of the three kinds of the order parameter textures; the A-phase texture, the singular vortex, and the half-quantum vortex for superfluid $^3\text{He-A}$ phase confined by narrow parallel plates with the radius R . After showing in §2 that the spinful singular vortex can accommodate the Majorana quasi-particle localized at the core, we examine the condition that the Majorana quasi-particle exists, namely, the stability of the singular vortex and also half-quantum vortex which is known to accommodate the Majorana quasi-particle.

We have found that under the external field applied to

either exactly parallel or perpendicular to the plates, the singular vortex state becomes stable above the critical rotation speed Ω_c which is evaluated. Thus the Majorana quasi-particles can be observed in those situation. The on-going experiment using the rotating cryostat at ISSP, Univ. Tokyo is particularly suited for this task because $\Omega_c \simeq 0.06$ rad/sec is within well controlled rotation speed. Moreover since singular vortex carries the Majorana quasi-particle localized at the core, we can design the braiding experiment by manipulating two or more Majorana quasi-particles.

Our calculations on the relative stability of the relevant textures are based on the standard Ginzburg-Landau functional which is firmly established through the cross checking between experiments and theories over several decades. Thus we believe that our results should be reliable not only qualitatively, but also quantitatively.

There are a few question remained to be clarified; (1) When the field is applied to exactly neither $\theta_H \neq 0$, or $\theta_H \neq \pi/2$, there appears the unwanted OP component $\Delta_{\uparrow\downarrow}$ whose magnitude is an order of 10^{-3} compared with the main component. At present we do not know whether or not this component is really harmful for the existence of the Majorana quasi-particle for the singular vortex. (2) We do not know how to take into account the so-called strong coupling effect in the gradient term in eq. (12) for general order parameter state. This remains a future problem.

In conclusion, independent of the above two reservations (1) and (2) we emphasize the fact that the parallel plate geometry whose gap is an order of $10 \mu\text{m}$ for superfluid $^3\text{He-A}$ phase is one of the best systems for detecting the Majorana quasi-particle.

Acknowledgments

We thank T. Mizushima and M. Ichioka for useful discussions.

- 1) L. Fu and C.L. Kane: Phys. Rev. Lett. **100** (2008) 096407.
- 2) P. Ghaemi and F. Wilczek: arXiv: 07092626.
- 3) J. Nilsson, A.R. Akhmerov and C.W.J. Beenakker: Phys. Rev. Lett. **101** (2008) 120403.
- 4) D.L. Bergman and K. Le Hur: Phys. Rev. B **79** (2009) 184520.
- 5) "Ettore Majorana", ed. by G.F. Bassani and the Council of the Italian Physical Society (Springer, Heidelberg, 2006).
- 6) D.A. Ivanov: Phys. Rev. Lett. **86** (2001) 268.
- 7) See for example, C. Nayak, S.H. Simon, A. Stern, M. Freedman, S. Das Sarma: Rev. Mod. Phys. **80** (2008) 1083.
- 8) T. Mizushima, M. Ichioka, and K. Machida: Phys. Rev. Lett. **101** (2008) 150409.
- 9) H-Y. Kee, Y.B. Kim, and K. Maki: Phys. Rev. B **62** (2000) R9275.
- 10) H-Y. Kee and K. Maki: Europhys. Lett. **80** (2007) 46003.
- 11) S. Das Sarma, C. Nayak, and S. Tewari: Phys. Rev. B **73** (2006) 220502(R).
- 12) S.B. Chung, H. Bluhm, and E-A. Kum: Phys. Rev. Lett. **99** (2007) 197002.
- 13) V. Vakaryuk, and A.J. Leggett: Phys. Rev. Lett. **103** (2009) 057003.
- 14) K. Machida and M. Ichioka: Phys. Rev. B **77** (2008) 184515.
- 15) A. G. Lebed and N. Hayashi: Physica C **341-348** (2000) 1677.
- 16) I. Zutic and I. Mazin: Phys. Rev. Lett. **95** (2005) 217004.
- 17) K. Machida, M. Ozaki, and T. Ohmi: J. Phys. Soc. Jpn. **58** (1989) 4116.

- 18) K. Machida, M. T. Nishira and T. Ohmi: J. Phys. Soc. Jpn. **68** (1999) 3364.
- 19) J.A. Sauls: Adv. Phys. **43** (1994) 113.
- 20) G.E. Volovik: JETP Lett. **70** (1999) 609-6114.
- 21) S. Tewari, S. Das Sarma, and D-H. Lee: Phys. Rev. Lett. **99** (2007) 037001.
- 22) A.J. Leggett: Rev. Mod. Phys. **47** (1975) 331.
- 23) D. Vollhardt and P. Wölfle: *The Superfluid phase of Helium 3* (Taylor and Francis, London, 1990).
- 24) G.E. Volovik and V.P. Mineev: JETP Lett. **24** (1976) 561.
- 25) M.C. Cross and W.F. Brinkman: J. Low Temp. Phys. **27** (1977) 683.
- 26) M.M. Salomaa and G.E. Volovik: Phys. Rev. Lett. **55** (1985) 1184.
- 27) M.M. Salomaa and G.E. Volovik: Rev. Mod. Phys. **59** (1987) 3533.
- 28) G.E. Volovik: *Exotic Properties of Superfluid ^3He* (World Scientific, Singapore, 1992) p.130.
- 29) M. Yamashita, K. Izumina, A. Matsubara, Y. Sasaki, O. Ishikawa T. Takagi, M. Kubota, and T. Mizusaki: Phys. Rev. Lett. **101** (2008) 025302.
- 30) T. Kawakami, Y. Tsutsumi and K. Machida: Phys. Rev. B **79** (2009) 092506.
- 31) Y. Tsutsumi, T. Kawakami, T. Mizushima, M. Ichioka and K. Machida: Phys. Rev. Lett. **101** (2008) 135302.
- 32) J.C. Wheatley: Rev. Mod. Phys. **47** (1975) 415.
- 33) J.A. Sauls and J.W. Serene: Phys. Rev. B **24** (1981) 183.
- 34) D.S. Greywall: Phys. Rev. B **33** (1986) 7520.
- 35) E.V. Thuneberg: Phys. Rev. B **36** (1987) 3583.
- 36) A.L. Fetter: in *Progress in Low Temperature Physics*, ed D.F. Brewer (Elsevier Science Publishers, Amsterdam, 1986) Vol. X, p. 1.
- 37) T. Kita: Phys. Rev. B **66** (2002) 224515.
- 38) V. Ambegaokar and N.D. Mermin: Phys. Rev. Lett. **30** (1973) 81.
- 39) The following GL parameters are used: $\alpha_0 = 3.81 \times 10^{50} [J^{-1}m^{-3}]$, and $\beta_1 = -3.75, \beta_2 = 6.65, \beta_3 = 6.56, \beta_4 = 5.99, \beta_5 = -8.53$ in units of $10^{99} [J^{-3}m^{-3}]$.